Alexandria Engineering Journal (2022) 61, 9427–9435

Alexandria University

Alexandria Engineering Journal

www.elsevier.com/locate/aej
www.sciencedirect.com

Low speed aerodynamic characteristics of non-slender delta wing at low angles of attack

Mohamed A. Mohamed [a,b], **Imran Afgan** [c,d], **Mohamed Hefny Salim** [e,f,*], **Ibrahim K. Mohamed** [g,f]

[a] *School of Engineering, University of South Wales, Pontypridd CF37 1DL, United Kingdom*
[b] *Faculty of Engineering, South Valley University, Qena 83523, Egypt*
[c] *School of MACE, The University of Manchester, Sackville Street, Manchester M13 9PL, United Kingdom*
[d] *Department of Mechanical Engineering, College of Engineering, Khalifa University, Abu Dhabi 127788, United Arab Emirates*
[e] *Geography Department, Humboldt-Universität zu Berlin, Berlin D-10099, Germany*
[f] *Faculty of Energy Engineering, Aswan University, Aswan 81528, Egypt*
[g] *Faculty of Engineering, King Abdulaziz University, Rabigh 21911, Saudi Arabia*

Received 31 July 2021; revised 27 February 2022; accepted 2 March 2022

KEYWORDS

Non-slender delta wing;
Half-span;
Subsonic wind tunnel;
Surface pressure measurements;
Aerodynamic characteristics

Abstract Low-speed wind tunnel experiments are conducted to study the aerodynamic performance of a half-span delta wing with 45° leading-edge sweep at subsonic flow regime. The experiments are carried out at a Reynolds number of 8.37×10^5, a free-stream Mach number of 0.1 and angles of attack up to 25°, in steps of 5°. The test model was designed with thirty-two pressure taps fixed on its surfaces (sixteen on each side). Multi-tube manometers were connected to these taps using long tubes to enable recording the pressure readings. Surface pressure distributions and aerodynamic characteristics were calculated at different span-wise locations along the non-dimensional chord-wise distance. Results exhibited that most lift on the studied wing is generated in the region close to the leading edge for all the studied incidence angles. Additional lift is created in the region close to the root chord rather than the tip chord, whereas drag forces increases from tip to root. This can be attributed to the formation of trailing edge vortexes due to the flow separation at the wing leading edge that produces more drag, hence suppressing lift. The study showed also that angle of attack increases the drag coefficient from tip to root, especially at high angle of attack, indicating unfavourable behaviour for manoeuvring. Moreover, the angle of attack increased the pitching moment coefficient up to 10° before it drops sharply until it reaches the tip of the wing model.

1. Introduction

Aircraft designed for supersonic flight are required to have high levels of manoeuvrability and controllability for effective

* Corresponding author at: Geography Department, Humboldt-Universität zu Berlin, Berlin D-10099, Germany.
E-mail address: mohamed.salim@geo.hu-berlin.de (M.H. Salim).
Peer review under responsibility of Faculty of Engineering, Alexandria University.

https://doi.org/10.1016/j.aej.2022.03.003
1110-0168

use in a combat arena. These aircrafts are usually equipped with thin, highly swept delta wings for reducing the supersonic wave drag and improving their supersonic cruise performance. However, the aerodynamic behaviour of swept delta wings is significantly different from the conventional wings at subsonic flow regime, in a way that the wing experiences poor performance [1].

For example, at low angles of attack, delta wings exhibit a severe drop in lift compared to the conventional wings, due to the absence of leading-edge vortexes (LEV). As the angle of attack increases, in take-off and landing phase, the sharp edges prevent the flow to remain attached to the surface and, consequently, the flow separates forming an unsteady separation bubble. This results in sever drag penalties and lateral control deficiencies [2].

The pressure difference between the upper and lower surfaces generates a vortical flow around the leading edges, which have crucial effect on the performance of the supersonic aircraft. The vortical flow detaches along the leading-edge towards the shear layer and curls up into two primary vortexes, as shown in Fig. 1. The strength and stability of these vortexes depends on the Reynolds number, the sweep angle, the slenderness, the leading edge sharpness and the angle of attack [3].

At moderate-to-high angles of attack, these vortexes induce additional velocity on the upper surface of the wing, hence reducing the pressure considerably. Consequently, an additional lift known as the vortex-lift will be provided. The benefit of this vortical flow has been directed towards military applications to enhance the transonic manoeuvrability, hence achieving high lift during take-off and landing [5]. As the angle of attack increases, the leading-edge vortexes experience a sudden disorganization, leads to vortex breakdown, hence, a dramatic expansion of the vortex core.

The primary vortexes burst far downstream of the trailing edge and the burst point travels upstream as the angle of attack increases. When the burst point approaches the wing trailing edge, the forward progression of core breakdown become more rapid and decreases as it reaches the apex of the wing. This in turn will lead to strong oscillation of the wing surface pressure downstream of the breakdown point and might lead to buffeting, hence deteriorating the aircraft performance [6].

The development of advanced fighter planes has generated a great interest towards the investigation of delta wings to improve the aerodynamic and control characteristics at high angles of attack [7]. Therefore, the study of vortical flow field around delta wings has been a subject of study for many researchers due to its essential applications to design of highly manoeuvrable aircrafts [8,9]. Numerous experimental studies have been conducted to understand the flow structure, aerodynamic characteristics and vortex breakdown phenomenon over delta wings of combat aircraft that flying at high angles of attack. For instance, Furman and Breitsamter [10] reported the experimental results on a 65° swept delta wing as part of the International Vortex Flow Experiment. Panyne et al. [11] showed that the core flow transforms into a wake-like flow from a jet-like flow when breakdown occurs. Instantaneous three-dimensional vorticity measurements in vortical flow over a delta wing are reported by Honkan and Andreopoulos [12]. Gad-el-Hak and Ho [13] carried out experiments to visualize the flow fields around two pitching delta wings with apex angles of 90 and 60°. Moreover, a considerable amount of literature has been published on the experimental investigation of flow and aerodynamics over delta wings [14–18]. These studies confirmed the importance of carrying out experimental studies on delta wings to understand the flow structure.

Furthermore, simulation methods accurately predicted the unsteady vortical flow, aerodynamics characteristics and the flow field around delta wings with blunt leading edge at realistic Reynolds numbers of full scale vehicles. Grtz and Rizzi [19] investigated the influence of viscosity on vortex breakdown. The leading-edge shape effect on the vortex flow over non-slender delta wings was provided by Elsayed et al. [20]. Mitchell et al. [21] analyzed the delta-wing vortical substructures using Detached-Eddy Simulation (DES) to alleviate the costly near-wall meshing requirements. Cummings and Schtte [22] also used the same technique, i.e. DES, to simulate the vortical flow field about the vfe-2 delta wing. Numerous studies have been conducted using both experimental and numerical approaches to investigate the aerodynamic characteristics and vortical flow structures over sharp edged slender delta wings with different sweep angles [23–28].

Over the past fifty years, extensive studies have been performed on the so-called slender delta wings ($\Lambda \geqslant 60°$), where the flow phenomena over these types of wings has been well understood [5,29]. On the other hand, the flow over non-slender delta wings $\Lambda < 60°$) has received less attention in the literature until recently. The early studies for the non-slender delta wings revealed that the vortex breakdown was

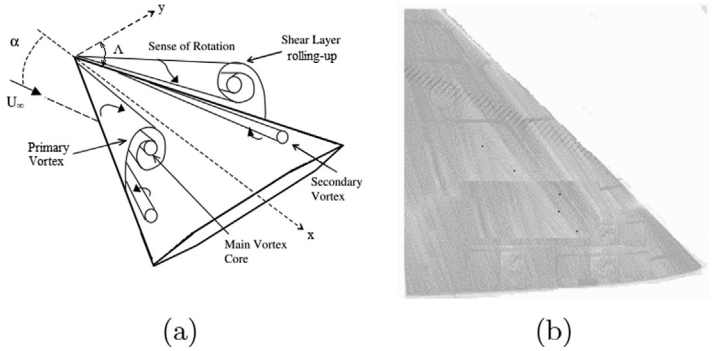

Fig. 1 (a) Schematic view of the flow structure over delta wing with sharp leading edge [4] (b) Wind-tunnel model of half-span delta wing with 45° lea.ding-edge sweep.

difficult to identify for sweep angles of 55° and 45° and it is not known whether the vortex breakdown is the main source of buffeting or not. However, the effect of leading edge radius on the flow structures over 50° swept delta wing was studied experimentally using an oil-flow visualization and a Stereo Particle Image Velocimetry (SPIV) technique [30]. The results showed that the leading-edge radius has crucial effect on the strength of vortical flow structures and the location of vortex core breakdown over the studied models. Recently, the ground effect on the flow characteristics and aerodynamic performance of a non-slender delta wing during take-off and landing at low angles of attack was investigated experimentally using PIV technique [31] and numerically using artificial intelligence techniques [32].

Although delta wings were designed primarily for high speed flights, the present experimental study is performed at subsonic flow regime, since the supersonic aircraft would spend more time in that segment in the take-off and landing phase. Very little knowledge is available for the unsteady flow phenomena and surface pressure distributions over the non-slender delta wings at very low subsonic flow regime. In addition, all the existing data is very old and not reliable.

Therefore, the present study is motivated by an essential goal for carrying out extensive wind tunnel tests to a half span non-slender delta wing having 45° sweep at angles of attack up to 25°. The surface pressure measurements obtained on both the suction and pressure surfaces have been used in calculating the aerodynamic characteristics such as lift, drag, pitching moment and pressure coefficients. The results of this study will help to better understand the flow characteristics of the non-slender delta wing at low angles of attack. The results will also be very useful for validating numerical studies conducted on non-slender delta wing based on different turbulence models.

The remaining part of the paper proceeds as follows: Section 2 gives the details of the experimental set-up of the model and the instrumentation used in this study. Section 3 introduces the results and discusses the findings of the research. Finally, Section 4 presents the main conclusions derived from this study.

2. Experimental set-up

2.1. Subsonic wind tunnel

All the experiments were conducted in a compact and practical subsonic open circuit wind tunnel type with a rectangular test section size of 0.762 m × 0.762 m and can handle free stream velocities in the range of 0.0 to 36 ms^{-1}. Figure 2a shows a schematic layout of the used open circuit wind tunnel with names of the main components. All necessary equipment that used for changing the angle of attack of test model in the pitch plane, measuring the aerodynamic forces and measuring surface pressure distributions was fitted to the sides of the wind tunnel working section. As illustrated the photo in Fig. 2b, the tunnel is equipped at the back with an AC three-phase axial variable speed fan, which draws the air into the inlet that is fitted with a honeycomb and multiple screens to streamline the flow hence reducing turbulence. The air then passes through the contraction cone prior to reach the test section, where the test model is mounted. Finally, the air passes through the diffuser at the end of the test section, and then back to the atmosphere. The turbulence level does not exceed more than 0.051% for a free-stream velocity at 10 ms^{-1}, except for regions very close to the tunnel walls with the variation of the free-stream velocity direction will be within ±0.6°.

2.2. Half-span delta wing (test model)

The test model used in the present set of measurements is a half-span symmetrical delta wing which has a tip chord greater than 0.0 m (cropped delta). A plate of aluminium was machined to form the shape of the test model with coordinates generated using a CAD software. A centre circular hole and a circular disc were fabricated to enable the test model to be securely mounted yet freely rotatable within the test section of the wind tunnel. The maximum thickness of the model after finishing was $t_{max} = 0.08$ m. The model had a leading-edge sweep of $\Lambda = 45°$ with a base width (semi-span) of $s/2 = 0.6$ m. The model had a root chord of $c_r = 0.7$ m and a tip chord of $c_t = 0.1$ m, while the radius of the leading-edge at root and tip were $R_{L.E(root)} = 0.075$ m and $R_{L.E(tip)} = 0.095$ m, respectively. At the trailing-edge, the model is bevelled on the windward side at an angle of $\beta = 20°$ to form sharp leading edges. A schematic diagram of the test model is shown in Fig. 3 with the geometric details listed in Table 1. In the present study, x represents the coordinate along the wing centre-line measured from the wing apex, y represents the coordinate along the wing local semi-span measured from the wing centre-line and z represents the height above the upper wing surface, as shown in Fig. 3.

2.3. Test conditions and accuracy

From a measurement of the Pitot and static pressures, the free-stream velocity upstream of the model was $U_\infty = 30\ ms^{-1}$, which gives a Reynolds number of $Re_c = 8.37 \times 10^5$ based on the mean aerodynamic chord of the test model. The free-stream velocity is estimated to have an accuracy of ±1%, while the mean intensity of turbulence was approximately 1%. The temperature of the ambient air was at $T_{amb.} = 40°C$, with an accuracy of ±2%, and the ambient air pressure was at $P_{amb.} = 1.01325 \times 10^5 Pa$ within ±2%.

Since the wind tunnel velocity was not varied, the free-stream Mach number was constant for all the wind tunnel testing experiments ($M_\infty = 0.1$). The model was mounted on a sting with a horizontal support and flexible joint for adjusting the angle of attack. A vertical column was used for manipulating the height of the horizontal support whilst constraining the model to remain aligned with the central axis of the test section. The test conditions for the present work covered a range of angles of attack from 0° to 25°, with an accuracy of ±0.05°. The test model was mounted in the test section with no yawing angle with respect to the free-stream flow with an accuracy of ±0.01°.

The overall uncertainty (w_R) of the experiment was calculated by Eq. 1 [33] by summing the uncertainties in each individual variable as indicated in Table 2. Based on Eq. 1 and the values in Table 2, w_R reached 10.18%.

$$w_R = \sqrt{u_\alpha^2 + u_{C_p}^2 + u_{C_L}^2 + u_{C_D}^2 + u_{C_{M.L.E}}^2} \quad (1)$$

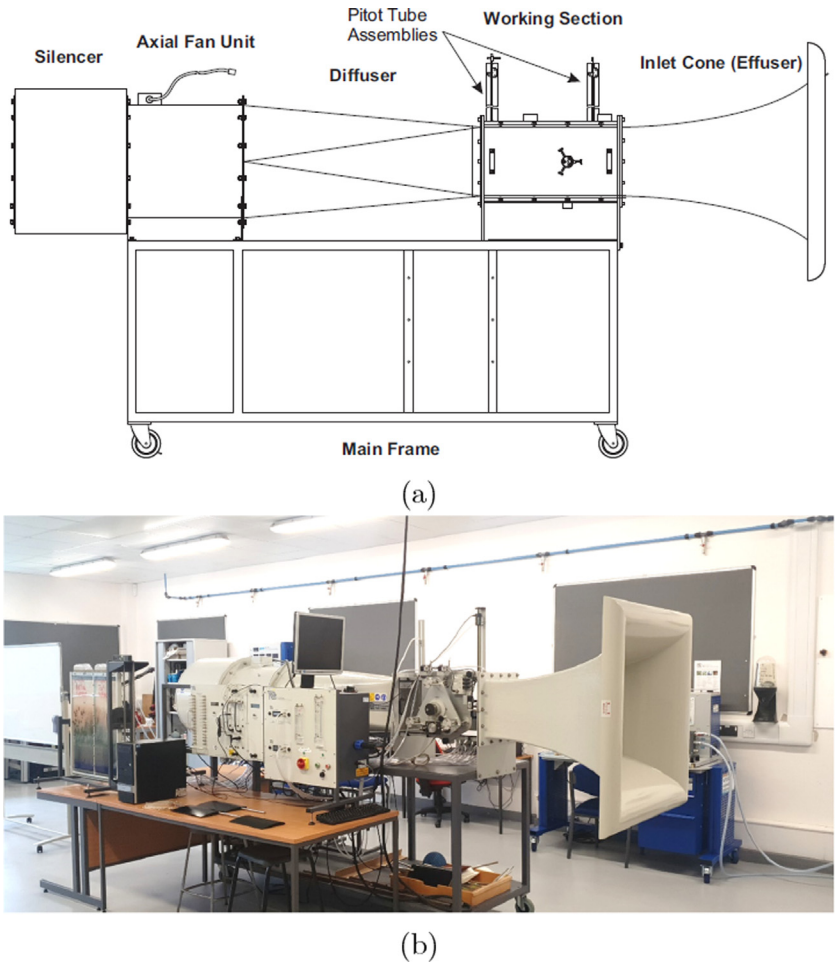

Fig. 2 Illustration of the subsonic wind-tunnel experimental facility showing (a) a schematic sketch and (b) a photo showing the actual view of the wind-tunnel.

2.4. Surface pressure measurements

Thirty-two pressure-tapping holes (0.8 mm inner diameter) were created on the test model to measure the surface pressure distributions at five span-wise locations. Twenty-six pressure tappings were scattered across each of the pressure and suction sides with 3 tapings on the leading edge and 3 on the trailing edge (see Fig. 4 for a schematic diagram for the location of the pressure tappings).

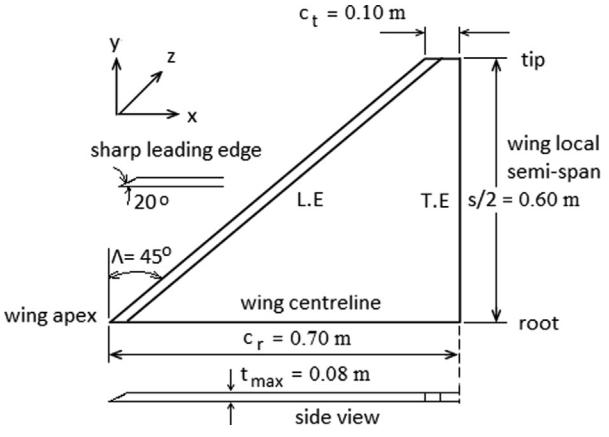

Fig. 3 Layout of the half-span delta wing geometry.

Table 1 Geometric details of half-span delta wing (test model).

Model parameters	Value
Root cord	$c_r = 0.7$ m
Tip cord	$c_t = 0.1$ m
L.E. radius at the root	$R_{L.E(root)} = 0.075$ m
L.E. radius at the tip	$R_{L.E(tip)} = 0.095$ m
Sweep angle	$\Lambda = 45^\circ$
Bevel angle	$\beta = 20^\circ$
Half-span	$s/2 = 0.6$ m
Max thickness	$t_{max} = 0.08$ m
Planform area	$A = s(c_r + c_t)/4 = 0.24$ m^2
Aspect Ratio	$AR = (s/2)^2/A = 1.5$
Taper Ratio	$\lambda = c_{tip}/c_{root} = 0.143$
Mean aerodynamic chord	$c_{mac} = 2/3c_r[(1 + \lambda + \lambda^2)/(1 + \lambda)] = 0.475$ m

Table 2 Uncertainty of the experiment variables.

Variable	Uncertainty
Angles of Attack	$\alpha = \pm 5\%$
Pressure Coefficient	$C_p = \pm 5\%$
Lift Coefficient	$C_L = \pm 4\%$
Drag Coefficient	$C_D = \pm 4\%$
Pitching Moment Coefficient	$C_{M,L.E} = \pm 4.65\%$

Two multi-tube manometers were connected to the pressure holes to record the pressure data from all pressure taps at the same time. To collect the surface pressure and velocity data, the test model was aligned in the test section at a geometric setting of zero angle of attack. The upper and lower surface pressure readings were matched to check if the test model was aerodynamically set at zero angle of attack or not. From the surface pressure data, the aerodynamic forces were calculated at angles of attack between 0° to 25°, in increments of 5°. The overall accuracy of pressure measurement was estimated to be less than 5%; the repeated tests indicated an uncertainty in the pressure coefficient of ±0.05. The wind tunnel was run up to a speed that indicated around 40 mm of water on Betz Micromanometer. The two reference pressures (P_A & P_B) of the wind tunnel, laboratory ambient pressure and ambient temperature, were recorded. The parameters of the free-stream conditions were calculated experimentally using the reference pressures and calibration constants ($K1$ & $K2$) of the wind tunnel [34].

3. Results and discussion

3.1. Pressure coefficients

Using the manometer height data from the two multi-tube manometers, the pressure distribution on both the upper and lower surfaces of the test model at the five span-wise stations were calculated and displayed in the form of graphs at angles of attack up to 25°, as shown in Figs. 5a-f. The flow around the non-slender half-span delta wing is assumed to be incompressible, inviscid and irrotational for low subsonic flow ($M_\infty < 0.3$). Bernoulis equation ($P + \rho V^2 = \text{constant}$) is applied at every point throughout an irrotational flow when a steady flow is assumed. From the measurements, the Pitot pressure is (P_0) and static pressure is (P_1), thus the velocity of air flow around the wing model is given by:

$$U = \sqrt{2(P_0 - P_1)/P_0} \tag{2}$$

The Pressure coefficient (C_P) is given by:

$$C_P = (P_1 - P_\infty)/q_\infty \tag{3}$$

where q_∞ is the dynamic pressure and is given by ($q_\infty = \rho_\infty V_\infty^2/2$). The two reference pressures P_A and P_B were calibrated so that dynamic and free-stream pressures at the test section can be calculated as follows:

$$q_\infty = K_1(P_A - P_B) \tag{4}$$

$$P_\infty = P_B + K_2(P_A - P_B) \tag{5}$$

where K_1 and K_2 are the wind tunnel calibration constants and they are approximated to be equal to 1.05 and 0.0 respectively.

As shown form Figs. 5a-f, a-f, the flow-induced pressure distributions were measured at five different span-wise values of y/s = 0.10, 0.35, 0.60, 0.85 and 0.95 along the non-dimensional chord-wise distance, x/c. From the pressure coefficient graphs, it can be seen that that most lift on the half-span span delta wing is generated in the region close to the leading edge for all the studied incidence angles.

The most aerodynamic aspect of delta wing is the formation of leading-edge vortexes that roll downstream over the wing suction side; hence trailing edge vortexes are dominating which causes more drag thereby suppressing lift. These stream-wise vortexes are formed due to the flow separation at the wing leading edge. As the flow separates, a vortex sheet rolls up into a vortex core where the flow accelerates as it travels downstream and finally it will be burst at some point downstream.

3.2. Lift coefficient at different angles of attack

The values of the lift coefficient (C_L) generated by the test model are calculated and compared at the five span-wise

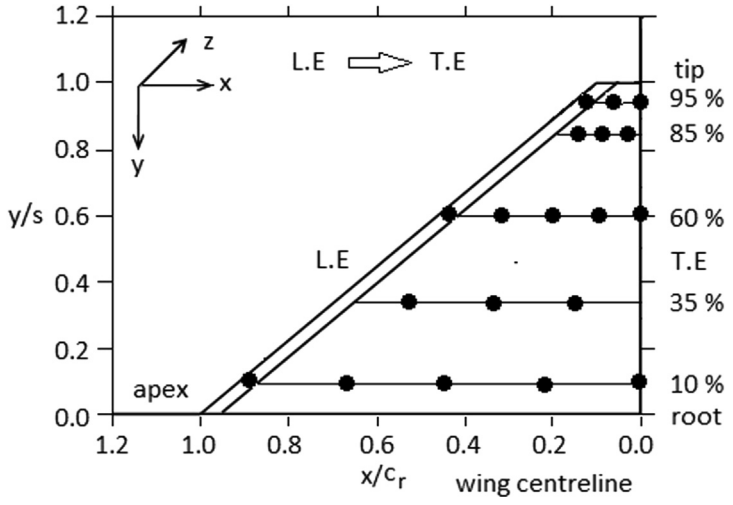

Fig. 4 Location of the pressure tapings on five span-wise stations starting from the root to tip.

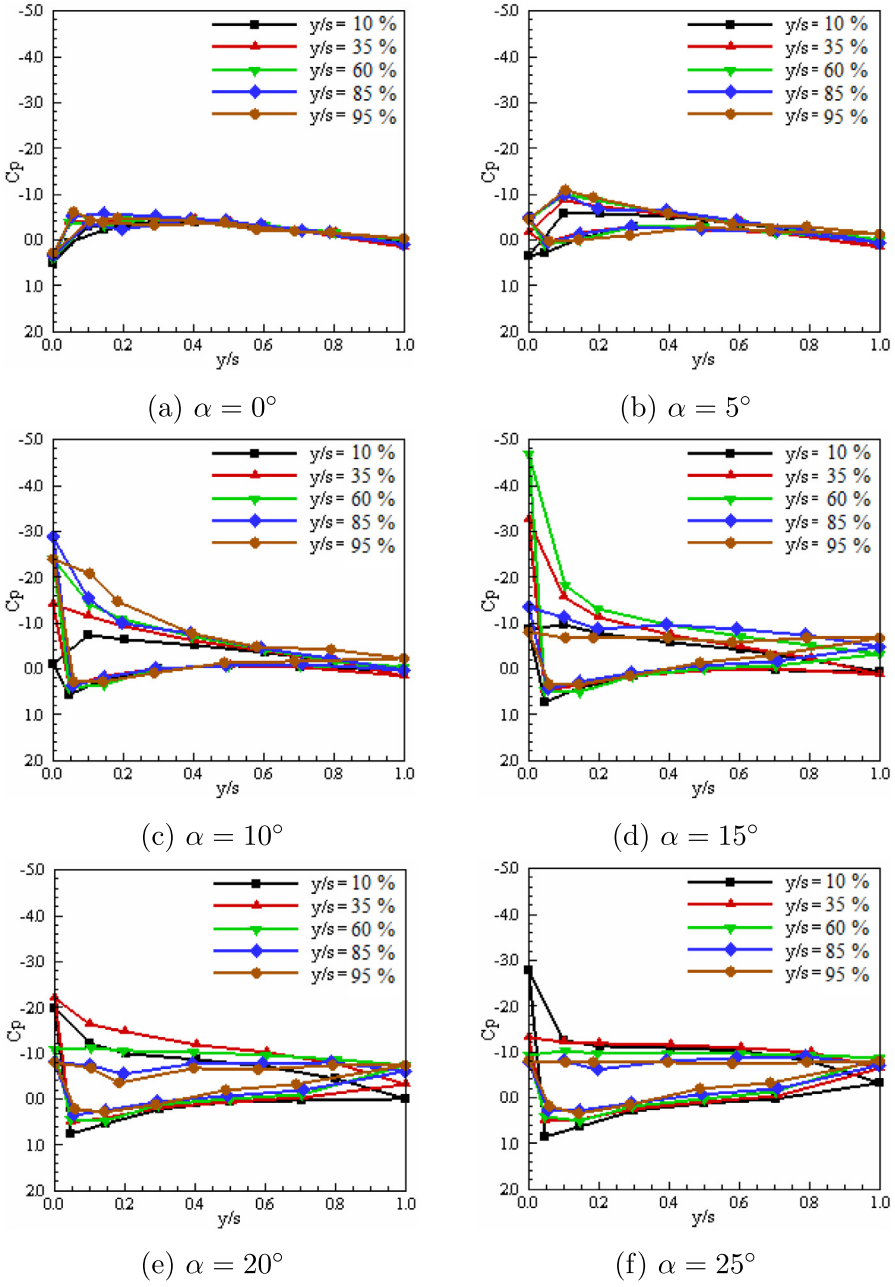

Fig. 5 Surface pressure distributions on the test model at five span-wise-stations.

stations in Fig. 6 at angles of attack $\alpha = 0°, \alpha = 5°, \alpha = 10°, \alpha = 15°, \alpha = 20°$ and $\alpha = 25°$.

Lift coefficient at each angle of attack is calculated using the following equation:

$$C_L = \frac{L}{(\rho V_\infty^2)/2)A} \tag{6}$$

The maximum uncertainty in lift coefficient calculations is found to be less than 4%.The graphs show that for $\alpha > 10°$ a higher lift is created in the region close to the root chord than that close to the tip chord (approximately 33%). Furthermore, lift increases slightly (approximately 5%) from chord to tip up to $\alpha = 10°$, then it starts to decrease as the angle of attack increases due to the vortex bursting which generates the drag. The angle of attack 10° represents here a turning angle after which the trend of the lift coefficient changes with cord length.

These results are generally inline with the delta wings related literature which showed that the local pressure decrease beneath the vortex core induces the vortex lift [35]. This local pressure increase has an intense acceleration of the longitudinal velocity. Also it was found that the upward deflected vortex flap (constant cord) could increase the lift coefficient by 0.18 at angle of attack before stall [36].

3.3. Drag coefficient at different angles of attack

Fig. 7 shows the plots of the drag coefficient (C_D) versus y/s at the range of the studied angles of attack, i.e. $\alpha = 0°$ to 25°. The

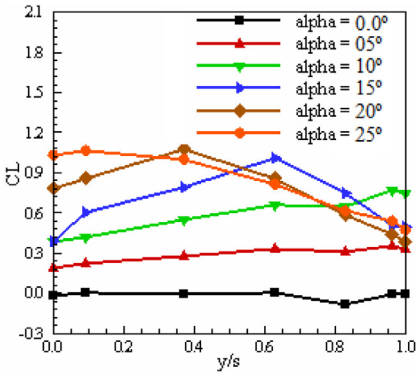

Fig. 6 Distribution of the lift coefficient on the test model against y/s at different angles of attack.

drag related to the skin friction is considered during the drag calculation since a thick boundary layer is developed due to the inviscid and the incompressible airflow around the test model.

The drag coefficient at each angle of attack is calculated using the following equation:

$$C_D = \frac{D}{(\rho V_\infty^2)/2)A} \tag{7}$$

The maximum uncertainty in drag coefficient calculations is found to be less than 4%. At very low angle of attach (α = 0° to 5°) the drag coefficient is very small. At these low angles, the skin friction is quite small due to the turbulent flow characteristics at low angle of attack. The angle of attach 10° represents a special case, similar to the lift coefficient results for this angle of attack. The drag coefficient slightly increased with the chord length. For $\alpha > 10°$, the drag coefficient rises with the angle of attack and this occurs from the tip to the root. The increasing drag coefficient at $\alpha > 10°$, is not surprising. It indicates the development of the thick boundary layer of this type of flow. This increase in the drag coefficient indicates a unfavourable behaviour for manoeuvring at $\alpha > 10°$.

This finding broadly supports the work of other studies which also reported increased drag coefficient with increasing

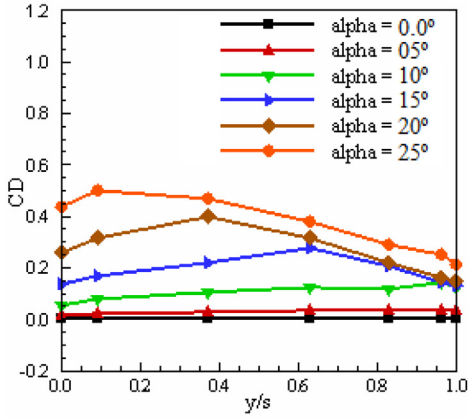

Fig. 7 Distribution of the drag coefficient on the test model against y/s at different angles of attack.

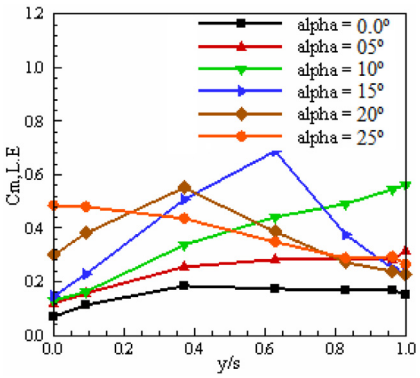

Fig. 8 Distribution of the Pitching moment coefficient about the leading edge on the test model against y/s at different angles of attack.

the angle of attack (see, e.g., Elsayed et al. [20] and Chen et al. [30]).

3.4. Pitching moment coefficient about the leading edge

The plots of the pitching moment coefficient about the leading edge, $C_{m,L.E}$ at five span-wise stations on the test model for studied angles of attack are shown in Fig. 8.

Pitching moment coefficient about the leading edge of the wing model is calculated from the following equation:

$$C_{M,L.E} = \frac{M}{(\rho V_\infty^2)/2)Ac_{MAC}} \tag{8}$$

The maximum uncertainty in $C_{M,L.E}$ calculations is found to be less than 4.65%. The plots show that the value of $C_{m,L.E}$ increases linearly from wing model root towards tip with the angle of attack up to $\alpha = 10°$, then it increases gradually for $\alpha = 15°$ & $\alpha = 20°$ until y/s = 0.37 & 0.63 respectively before it drops sharply until reaches the tip of the wing model. For $\alpha = 25°$, the moment coefficient become steady for the model root until $y/s = 0.09$, then starts to decrease slowly until the tip point.

The change in pitching moment slope for $\alpha = 25°$ indicates that the model gradually shifts from a statically stable configuration to a statically unstable configuration. Similar to the results of lift and drag coefficient, the trend of the pitching moment coefficient changed due to the development of the turbulent flow along the cord length with the relatively increase angle of attack.

The turbulent flows with leading edge vortexes at $\alpha = 25°$ might be generated over the delta wing in the post-stall regime. More information on the fluctuations of the pressure readings, and ultimately the lift, drag and pitching moment coefficients, could be usefully explored in further research. Due to the limitations of the study, further work needs to be done to establish quantitative observations and statistical analysis on these variables.

4. Conclusions

A comprehensive experimental study is presented in this paper to investigate the unsteady flow field and surface pressure dis-

tributions over a non-slender delta wing in the subsonic flow regime and angles of attack ranging from 0° to 25°. The measurements were taken at five different span-wise stations. The results showed that the generated lift on the non-slender delta wing mostly occurs in the region close to the leading edge and its value increases gradually with increasing the angle of attack. This is due to the formation of leading edge vortexes which generates an additional lift. The results showed also that at angle of attack greater than 10° the flow characteristics significantly changes. The drag coefficient increase after this angle, indicating unfavourable behaviour for manoeuvring after this angle of attack. Also, a higher lift is created in the region close to the root than the tip-chord. On the other hand the drag force increases with an increase in the angle of attack and from the tip to root of the wing. The increase of the drag force may reach 60% in case of angle of attack of 25°.

These findings contribute in several ways to our understanding of the aerodynamics of non-slender delta wing at low angle of attack. However, further numerical studies could assess the aerodynamics of these flows using computational fluid dynamics models based on advanced turbulence models. These proposed studies will benefit from the measurement reported in the current study. This would be a fruitful area for further work.

Declaration of Competing Interest

The authors declare that they have no known competing financial interests or personal relationships that could have appeared to influence the work reported in this paper.

Acknowledgment

The article processing charge was funded by the Deutsche Forschungsgemeinschaft (DFG, German Research Foundation) – 491192747 and the Open Access Publication Fund of Humboldt-Universität zu Berlin.

References

[1] I. Gursul, Review of unsteady vortex flows over slender delta wings, J. Aircraft 42 (2) (2005) 299–319.
[2] L.D. Luca, G. Guglieri, G. Cardone, G.M. Carlomagno, Experimental analysis of surface flow on a delta wing by infrared thermography, AIAA J. 33 (8) (1995) 1510–1512, https://doi.org/10.2514/3.12574.
[3] I. Gursul, R. Gordnier, M. Visbal, Unsteady aerodynamics of nonslender delta wings, Prog. Aerosp. Sci. 41 (7) (2005) 515–557.
[4] Z.F. Mahdavi, S.M. Reza, An experimental investigation of the vortex merging over a cranked-delta wing at subsonic speed, J. Aerospace Eng. Mech. 5 (1) (2021), https://doi.org/10.36959/422/453.
[5] M.D. Manshadi, M. Eilbeigi, M.K. Sobhani, M.B. Zadeh, M.A. Vaziry, Experimental study of flow field distribution over a generic cranked double delta wing, Chin. J. Aeronaut. 29 (5) (2016) 1196–1204, https://doi.org/10.1016/j.cja.2016.08.002.
[6] J.M. Rullan, The aerodynamics of low sweep delta wings, Thesis (2008).
[7] E.C. Polhamus, Applying slender wing benefits to military aircraft, J. Aircraft 21 (8) (1984) 545–559.
[8] F. Payne, T. Ng, R. Nelson, L. Schiff, Visualization and wake surveys of vortical flow over a delta wing, AIAA J. 26 (2) (1988) 137–143.
[9] J. Ekaterinaris, L. Schiff, Vortical flows over delta wings and numerical prediction of vortex breakdown, in: 28th Aerospace Sciences Meeting, 1990, p. 102.
[10] A. Furman, C. Breitsamter, Turbulent and unsteady flow characteristics of delta wing vortex systems, Aerosp. Sci. Technol. 24 (1) (2013) 32–44, https://doi.org/10.1016/j.ast.2012.08.007.
[11] F. Payne, T. Ng, R. Nelson, L. Schiff, Visualization and flow surveys of the leading edge vortex structure on delta wing planforms, in: 24th Aerospace Sciences Meeting, American Institute of Aeronautics and Astronautics, 1986. https://doi.org/10.2514/6.1986-330.
[12] A. Honkan, J. Andreopoulos, Instantaneous three-dimensional vorticity measurements in vortical flow over a delta wing, AIAA J. 35 (10) (1997) 1612–1620, https://doi.org/10.2514/2.20.
[13] M.G. el Hak, C.-M. Ho, The pitching delta wing, AIAA J. 23 (11) (1985) 1660–1665, https://doi.org/10.2514/3.9147.
[14] S. Mat, I.S. Ishak, T.M. Lazim, S. Mansor, M. Said, A.B.A. Rahman, A.S.M. Kamaludim, R. Brossay, Development of delta wing aerodynamics research in universiti teknologi malaysia low speed wind tunnel, Adv. Mech. Eng. 6 (2014) 434892, https://doi.org/10.1155/2014/434892.
[15] I. Gursul, M. Allan, K. Badcock, Opportunities for the integrated use of measurements and computations for the understanding of delta wing aerodynamics, Aerosp. Sci. Technol. 9 (3) (2005) 181–189, https://doi.org/10.1016/j.ast.2004.08.007.
[16] S.B. Mat, R. Green, R. Galbraith, F. Coton, The effect of edge profile on delta wing flow, Proc. Inst. Mech. Eng., Part G: J. Aerospace Eng. 230 (7) (2015) 1252–1262, https://doi.org/10.1177/0954410015606939.
[17] M.S. Ghazijahani, M.M. Yavuz, Effect of thickness-to-chord ratio on aerodynamics of non-slender delta wing, Aerosp. Sci. Technol. 88 (2019) 298–307, https://doi.org/10.1016/j.ast.2019.03.033.
[18] T. Lee, L. Ko, Vortex flow and lift generation of a non-slender reverse delta wing, Proc. Inst. Mech. Eng., Part G: J. Aerospace Eng. 231 (13) (2016) 2438–2451, https://doi.org/10.1177/0954410016671342.
[19] A. Rizzi, S. GOERTZ, K. Munukka, Computational study of vortex breakdown over swept delta wings, in: 17th Applied Aerodynamics Conference, American Institute of Aeronautics and Astronautics, 1999. https://doi.org/10.2514/6.1999-3118.
[20] M. Elsayed, F. Scarano, N. Verhaagen, Leading-edge shape effect on the vortex flow over non-slender delta wings, in: 46th AIAA Aerospace Sciences Meeting and Exhibit, American Institute of Aeronautics and Astronautics, 2008. https://doi.org/10.2514/6.2008-344.
[21] A.M. Mitchell, S.A. Morton, J.R. Forsythe, R.M. Cummings, Analysis of delta-wing vortical substructures using detached-eddy simulation, AIAA J. 44 (5) (2006) 964–972.
[22] R.M. Cummings, A. Schütte, Detached-eddy simulation of the vortical flow field about the vfe-2 delta wing, Aerosp. Sci. Technol. 24 (1) (2013) 66–76.
[23] R. Cummings, S. Morton, S. Siegel, Computational simulation and piv measurements of the laminar vortical flowfield for a delta wing at high angle of attack, in: 41st Aerospace Sciences Meeting and Exhibit, 2003, p. 1102.
[24] X. Meng, C. Jia, Z. Qiao, C. Gao, S. Luo, F. Liu, Aerodynamic characteristics of slender delta wing with low dorsal fin, in: 45th AIAA Aerospace Sciences Meeting and Exhibit, American Institute of Aeronautics and Astronautics, 2007. https://doi.org/10.2514/6.2007-1272.
[25] A. Oyama, G. Imai, A. Ogawa, K. Fujii, Aerodynamic characteristics of a delta wing at high angles of attack, in: 15th AIAA International Space Planes and Hypersonic Systems and Technologies Conference, 2008, p. 2563.

[26] A.Z. Al-Garni, F. Saeed, A.M. Al-Garni, Experimental and numerical investigation of 65 degree delta and 65/40 degree double-delta wings, J. Aircraft 45 (1) (2008) 71–76.
[27] S. Saha, B. Majumdar, Experimental and numerical study of surface flow pattern on delta wing, Int. J. Emerg. Technol. Adv. Eng. 2 (3) (2012) 215–222.
[28] H. Rahman, S. Khushnood, A. Raza, K. Ahmad, Experimental and computational investigation of delta wing aerodynamics, in: Proceedings of 2013 10th International Bhurban Conference on Applied Sciences & Technology (IBCAST), IEEE, 2013, pp. 203–208.
[29] N. Verhaagen, Effects of leading-edge radius on aerodynamic characteristics of 50 delta wings, in: 48th AIAA Aerospace Sciences Meeting Including the New Horizons Forum and Aerospace Exposition, 2010, p. 323.
[30] L. Chen, J. Wang, L. xuan Zuo, L.-H. Feng, Influence of reynolds number on vortex flow over a non-slender delta wing, AIAA J. 48 (12) (2010) 2831–2839, https://doi.org/10.2514/1.j050246.
[31] S. Tumse, M.O. Tasci, I. Karasu, B. Sahin, Effect of ground on flow characteristics and aerodynamic performance of a non-slender delta wing, Aerosp. Sci. Technol. 110 (2021) 106475, https://doi.org/10.1016/j.ast.2020.106475, URL: https://doi.org/10.1016/j.ast.2020.106475.
[32] S. Tumse, M. Bilgili, B. Sahin, Estimation of aerodynamic coefficients of a non-slender delta wing under ground effect using artificial intelligence techniques, Neural Comput. Appl. (2022), https://doi.org/10.1007/s00521-022-07013-x.
[33] P. Bevington, D.K. Robinson, Data Reduction and Error Analysis for the Physical Sciences, McGraw-Hill Education Ltd, 2002.
[34] .B. Barlow, W.H. Rae, A. Pope, Low-speed wind tunnel testing, John Wiley & Sons, 1999.
[35] M. Lee, C.-M. Ho, Lift force of delta wings, Appl. Mech. Rev. 43 (9) (1990) 209–221, https://doi.org/10.1115/1.3119169.
[36] J.F. Marchman, Aerodynamics of inverted leading-edge flaps on delta wings, J. Aircraft 18 (12) (1981) 1051–1056, https://doi.org/10.2514/3.57599.